

Supporting information:

Strengthened Cathode Interface by Ultrathin 2D Ferroelectric for Inverted Perovskite Solar Cells

Hua Zhang,^{a} Weihong Liu,^a Yongping Bao,^a Rong Wang,^a Jianfei Liang,^a Lei Wan,^b Huan Wang^{b*}*

Prof. H. Zhang, W. Liu, R. Wang, J. Liang

^a Institute of Physical Science and Information Technology, Anhui University, Hefei, 230601, China

Dr. L. Wan, Dr. H. Wang

^b School of Electrical Engineering and Automation, Hefei University of Technology, Hefei, 230009, China

*Corresponding authors. E-mail: zhanghua@ahu.edu.cn; wanghuan@hfut.edu.cn;

1. Supplementary Figures

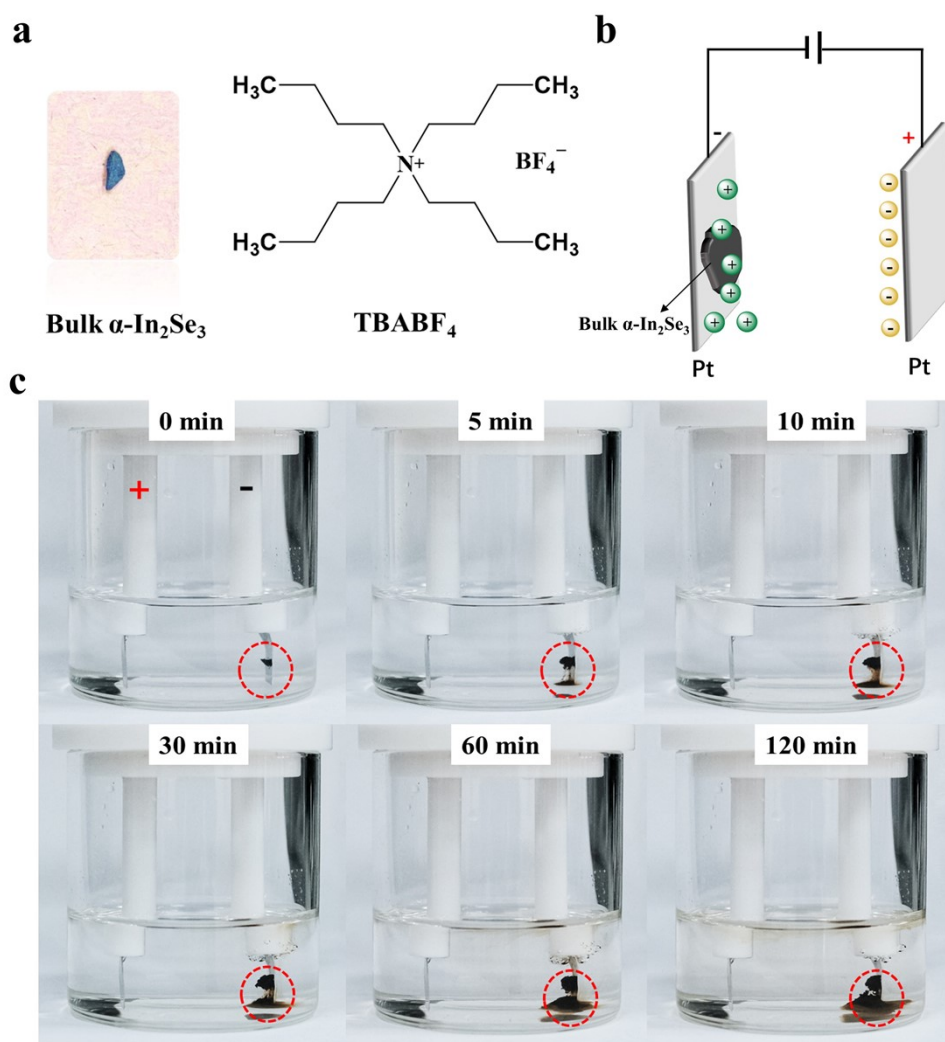


Figure S1 (a) Bulk α - In_2Se_3 crystal and intercalated molecules used in this work (b) Illustration of the exfoliation with two-electrode system (c) Optical images of the electrochemical exfoliation process ranging from 0 to 120 min.

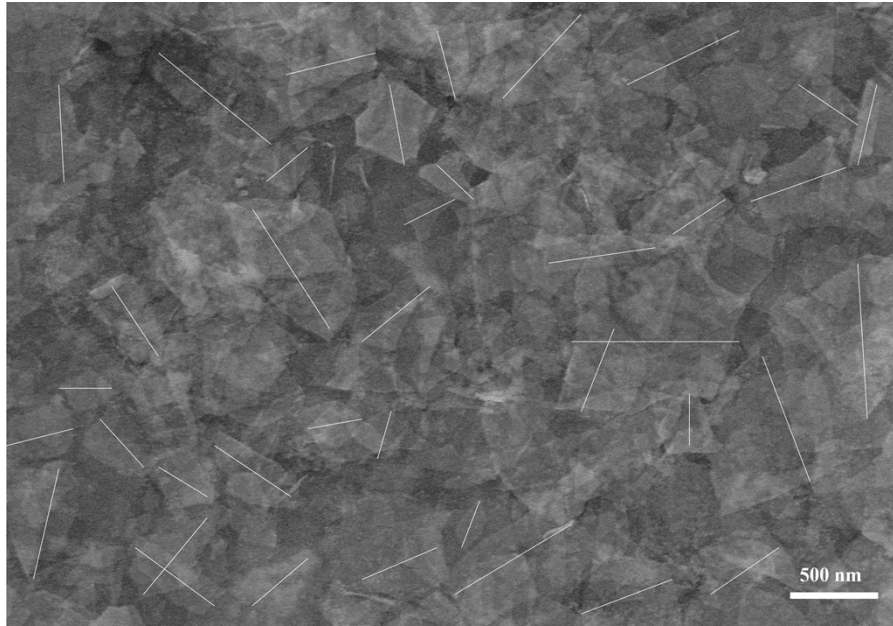


Figure S2 Typical SEM image of α -In₂Se₃ flakes taken from the supernatant.

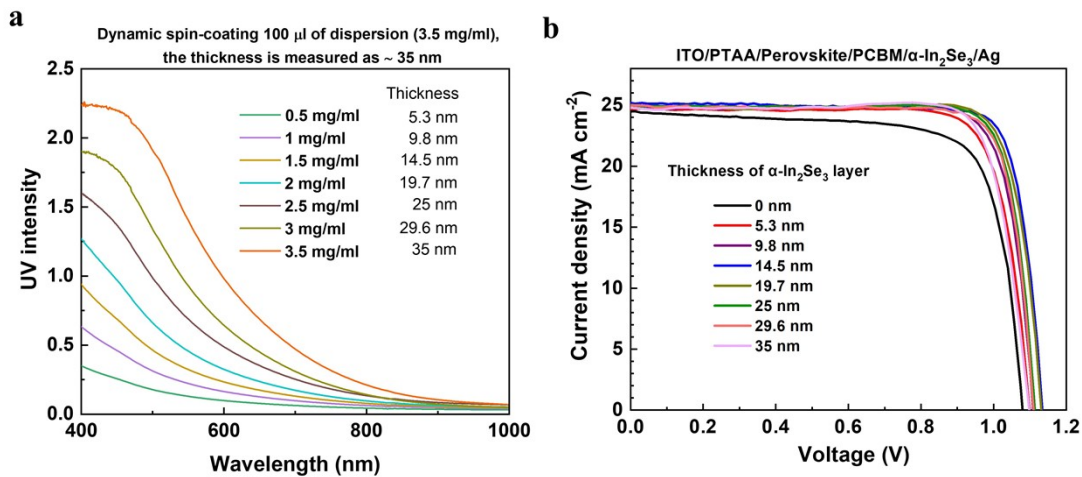


Figure S3 (a) Absorbance spectra and corresponding thicknesses of the α -In₂Se₃ films fabricated with different concentration. The thicknesses of the α -In₂Se₃ films were calculated by the relative absorption intensity for the thickness of thin film being proportional to UV absorption intensity. **(b)** The J-V curves of the devices with different thicknesses of α -In₂Se₃ layer ranging from 0 to 35 nm in reverse scan direction under standard AM 1.5G solar radiation.

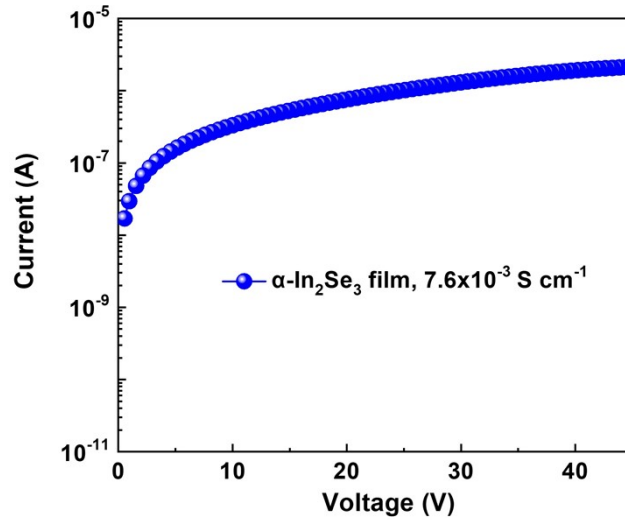


Figure S4 Electrical conductivity of α - In_2Se_3 film obtained from the bottom-up assembly of ultrathin α - In_2Se_3 flakes with the thickness around 95 nm.

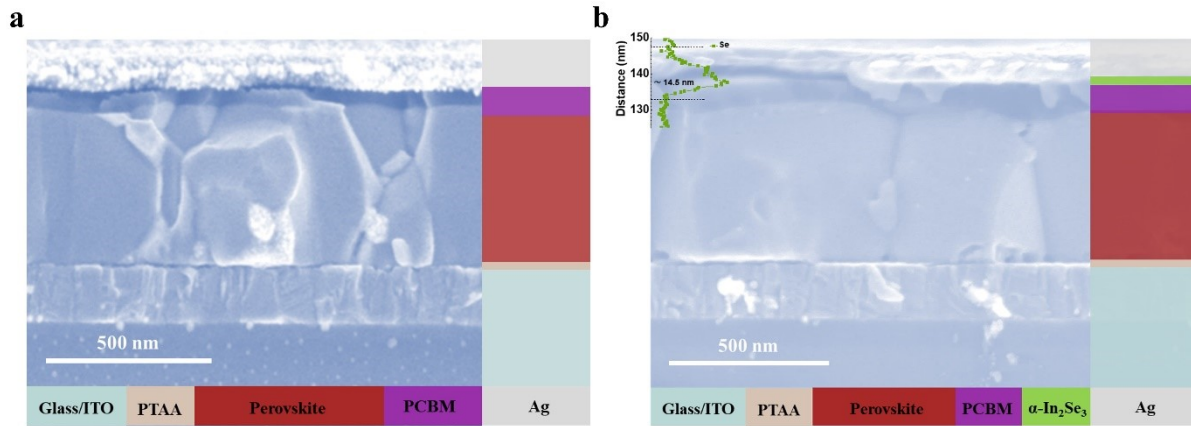


Figure S5 The typical cross-section SEM images of (a) the control device (b) the optimal device with α - In_2Se_3 layer. Inset is EDS line-scan profile of Se atom.

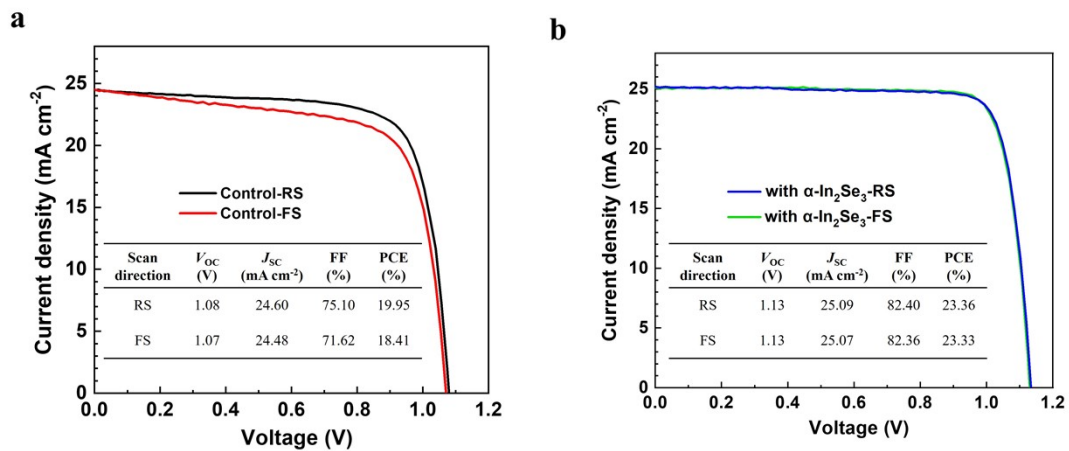


Figure S6 The J-V curves of (a) the best control device (b) the device with α - In_2Se_3 but no poling under standard AM 1.5G solar radiation.

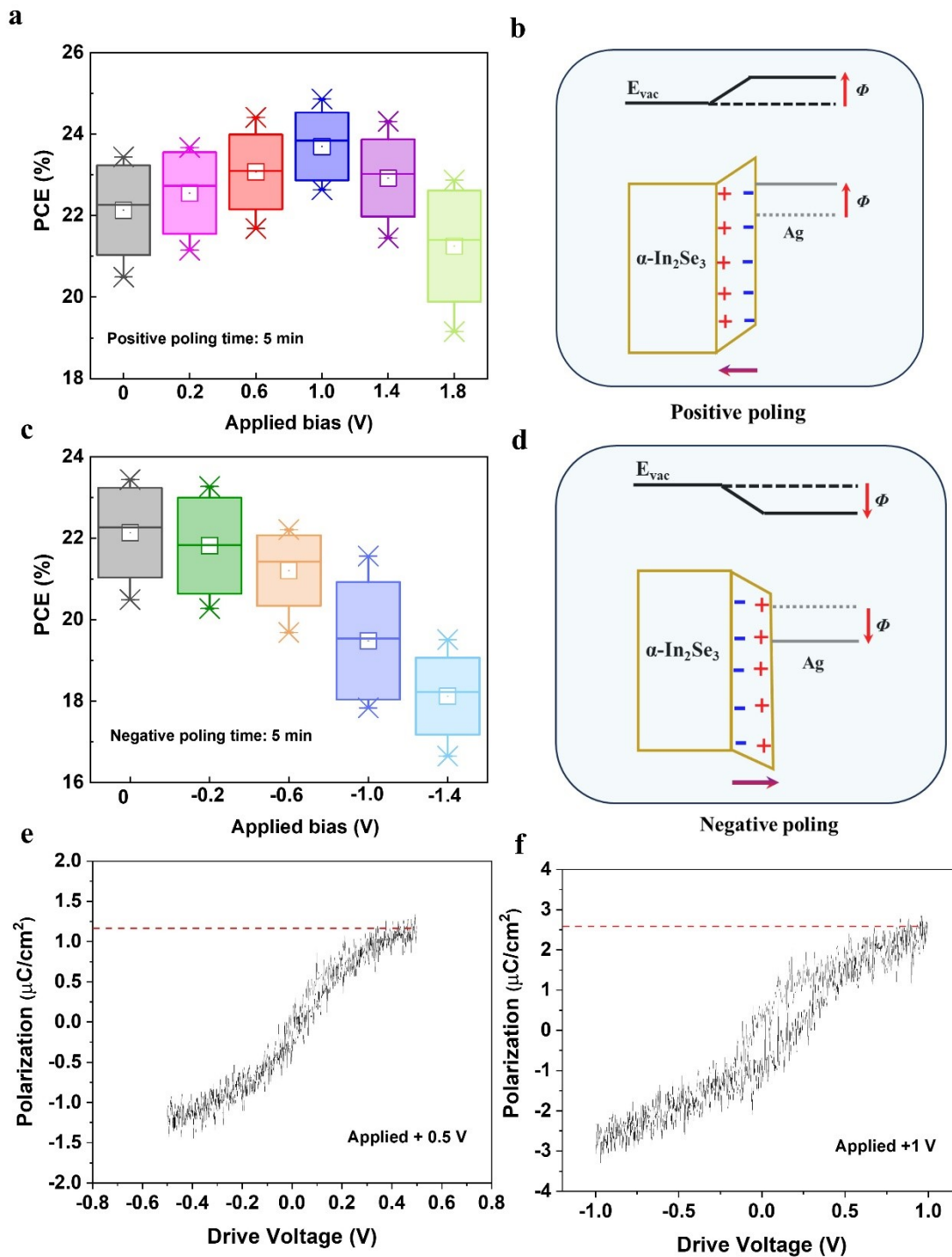


Figure S7 (a) PCE distribution of the $\alpha\text{-In}_2\text{Se}_3$ based devices under positive poling with the applied bias to Ag electrode ranging from 0 to 1.8 V (b) The corresponding energy level diagram at the $\alpha\text{-In}_2\text{Se}_3/\text{Ag}$ interface (c) PCE distribution of the $\alpha\text{-In}_2\text{Se}_3$ based devices under negative poling with the applied bias to Ag electrode ranging from 0 to -1.4 V (d) The corresponding energy level diagram at the $\alpha\text{-In}_2\text{Se}_3/\text{Ag}$ interface. P-V loops of the bare $\alpha\text{-In}_2\text{Se}_3$ film under an applied positive bias of (e) 0.5 V and (f) 1.0 V.

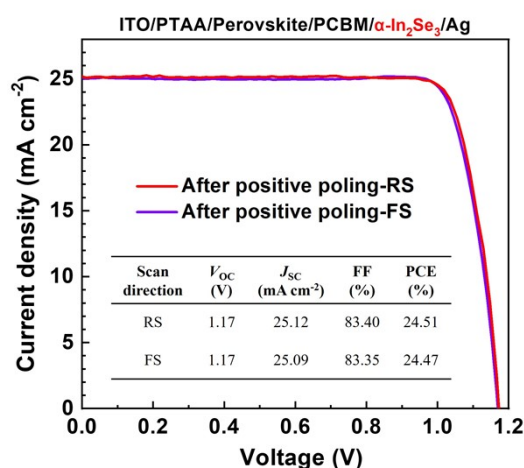


Figure S8 The J-V curve of the champion $\alpha\text{-In}_2\text{Se}_3$ based device after a positive poling (at +1 V for 5 min) under standard AM 1.5G solar radiation.

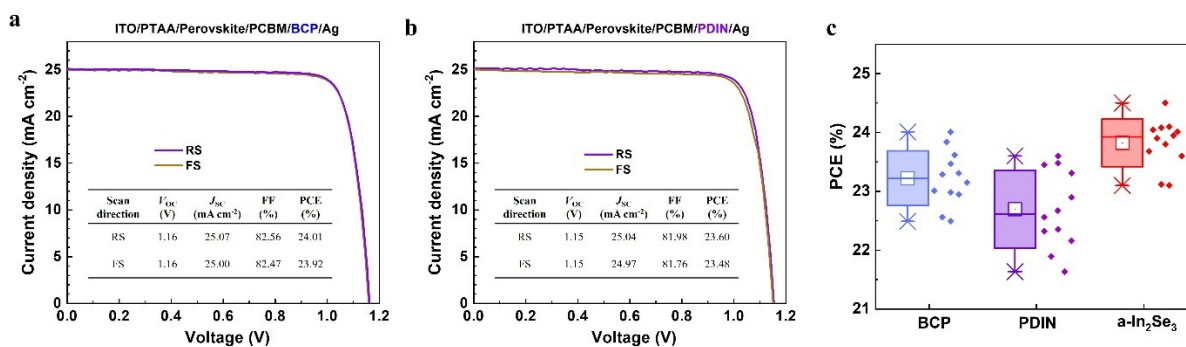


Figure S9 The J-V curves of the best-performing devices based on (a) thermal evaporated BCP as CBL (b) PDIN as CBL (c) the corresponding box chart of PCEs comparing with the $\alpha\text{-In}_2\text{Se}_3$ based device.

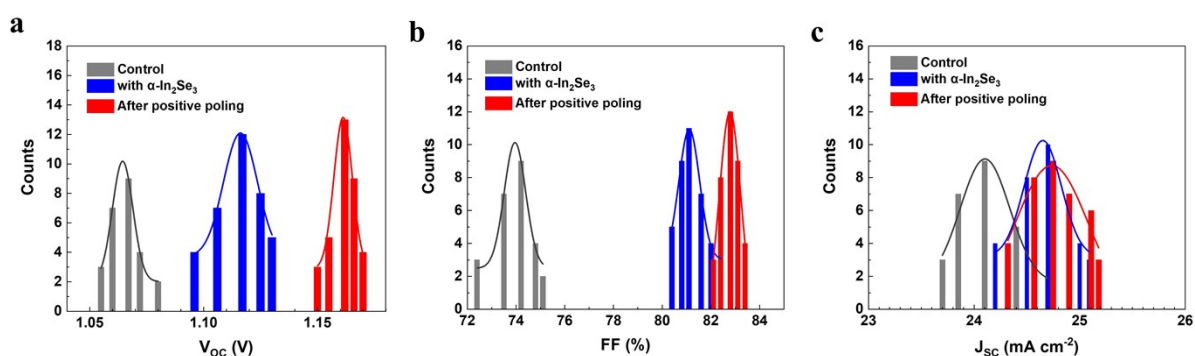


Figure S10 (a)-(c) Photovoltaic parameters (V_{oc} , FF and J_{sc}) statistic of the control devices, the $\alpha\text{-In}_2\text{Se}_3$ based devices before and after a positive poling.

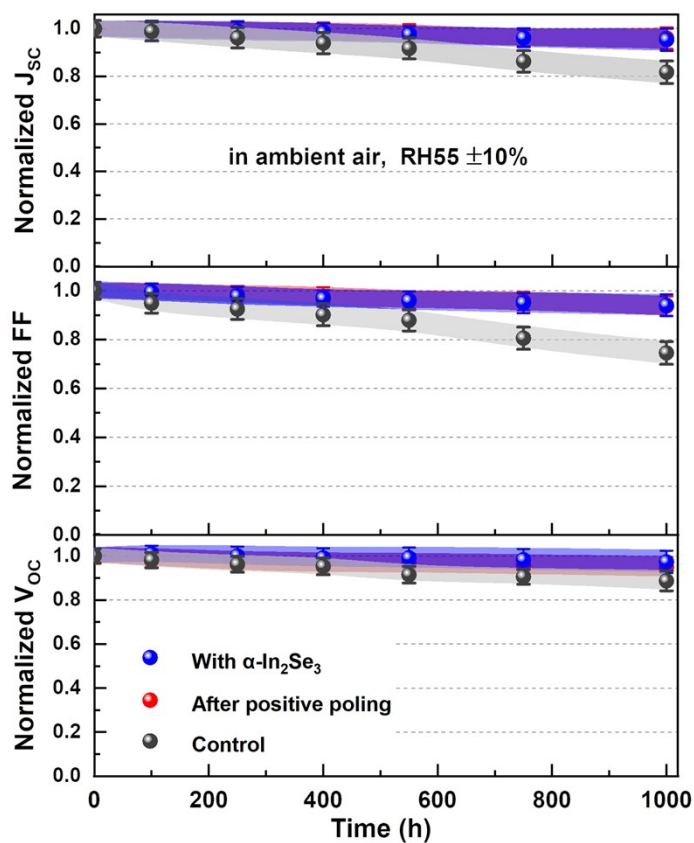


Figure S11 Evolution of normalized performance parameters of unsealed devices measured in ambient air with RH of $55 \pm 10\%$. The error bars represent the standard deviation from 4 cells for each type.

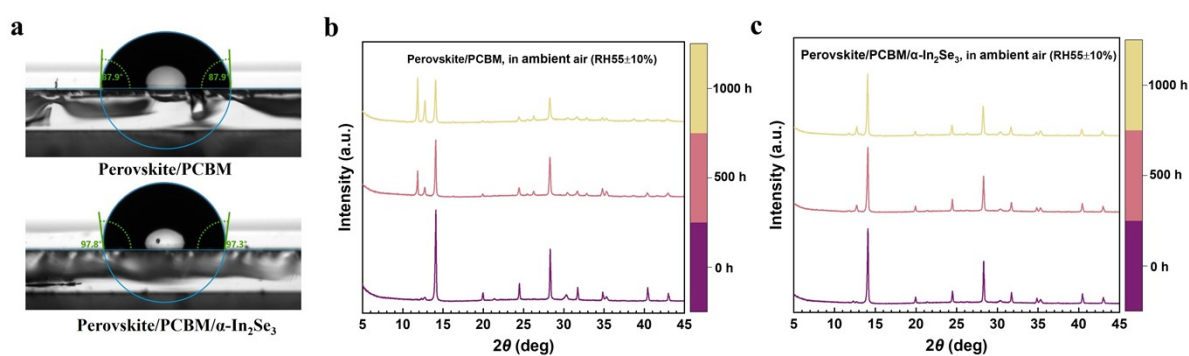


Figure S12 (a) The water contact angles of the perovskite/PCBM and perovskite/PCBM/ α - In_2Se_3 films (b)-(c) The corresponding aged XRD measurements, in which the stacks were stored under dark in ambient air with $\text{RH} 55 \pm 10\%$.

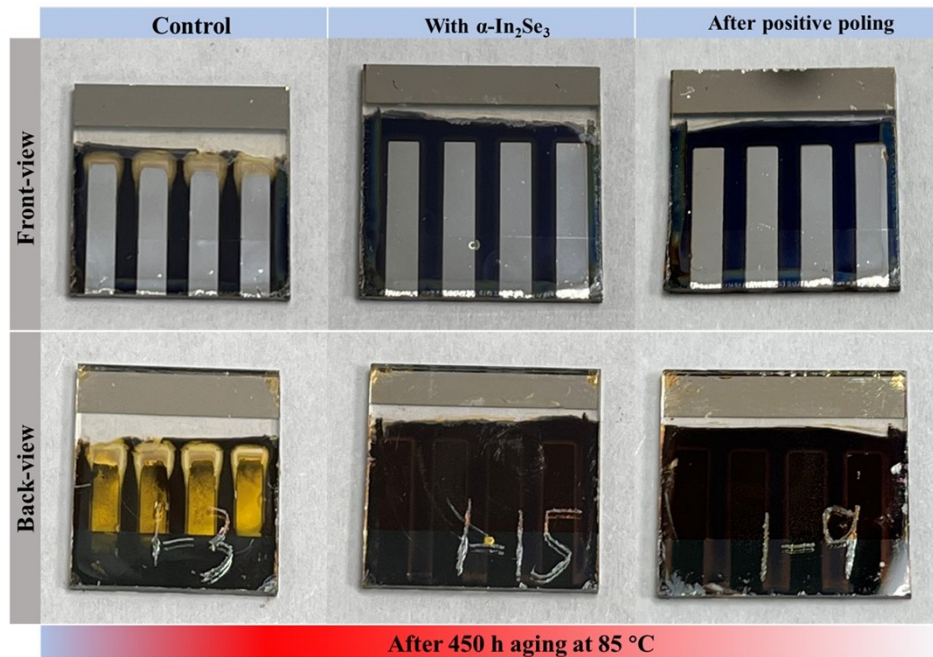


Figure S13 Optical images of three types of devices after aging at 85°C for 450 h. For the control device, it can be seen that the thermal-annealing accelerated ion migration, leading to a corroded Ag electrode and loss its metallic luster from the front-view, while the back-view clearly reveals the color change, implying the device degradation. In contrast, the α - In_2Se_3 based devices, before and after poling, both maintain good metallic luster of Ag electrode and no obvious color changes were observed during the same aging period, supporting the effective suppression of electrode corrosion and device degradation associated with ion migration.

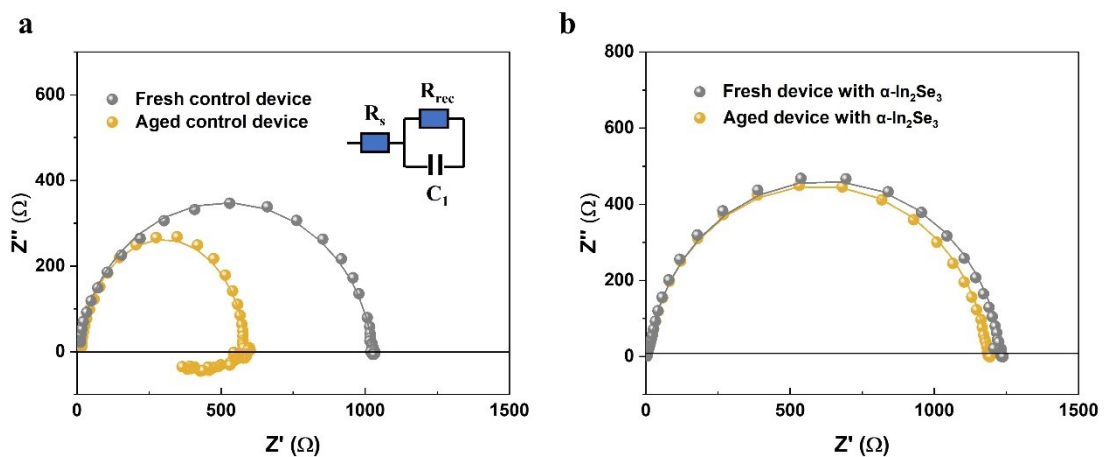


Figure S14 Nyquist plots of PSCs at 0.5 V in dark (a) the control device before and after aging under heat-light soaking conditions, the inset is the equivalent circuit used for curve fitting. (b) the α - In_2Se_3 based devices under the same conditions.

2. Supplementary Tables

Table S1. Extracted TRPL lifetime by fitting the curves with a bi-exponential function $I(t) = A_1 \exp(-t/\tau_1) + A_2 \exp(-t/\tau_2)$, and $\tau_{\text{avg}} = \tau_1 \times (A_1/A_1+A_2) + \tau_2 \times (A_2/A_1+A_2)$.

Samples	A ₁ %	τ_1 (ns)	A ₂ %	τ_2 (ns)	τ_{avg} (ns)
Perovskite/PCBM/Ag	41.9%	1.13	58.1%	20.79	12.55
Perovskite/PCBM/ α -In ₂ Se ₃ /Ag (no poling)	44.8%	1.32	55.2%	9.08	5.60
Perovskite/PCBM/ α -In ₂ Se ₃ /Ag (negative poling)	46.3%	1.37	53.7%	15.45	8.93
Perovskite/PCBM/ α -In ₂ Se ₃ /Ag (positive poling)	22.1%	0.67	77.9%	4.63	3.76

Table S2 The dependence of device performance on the thickness of α -In₂Se₃ layer. The photovoltaic parameters were extracted from J-V curves in reverse scan direction under the illumination of AM 1.5G, 100 mW cm⁻².

Thickness of α -In ₂ Se ₃ layer	V _{OC} (V)	J _{SC} (mA cm ⁻²)	FF (%)	PCE (%)	R _{sh} (Ω cm ⁻²)	R _s (Ω cm ⁻²)
0	1.08	24.60	75.10	19.95	9.6k	12.5
5.3	1.10	24.72	79.88	21.72	10.5k	10.3
9.8	1.11	24.85	82.26	22.69	11.4k	7.8
14.5	1.13	25.09	82.40	23.36	12.7k	7.2
19.7	1.13	25.00	82.51	23.31	12.6k	7.0
25	1.12	24.97	83.06	23.23	11.8k	7.4
29.6	1.12	24.91	82.08	22.90	11.5k	8.1
35	1.10	24.85	81.87	22.38	10.6k	9.7

Table S3. Summarized J-V characteristics of the unsealed control device during the operational stability test. The curves were recorded at a scan rate of 0.01 V s⁻¹ in reverse mode.

Time (h)	V _{OC} (V)	J _{SC} (mA cm ⁻²)	FF (%)	PCE (%)
0	1.06	24.48	76.00	19.72
24	1.06	24.37	76.95	19.88
72	1.05	23.75	76.31	19.03
150	1.05	23.11	75.65	18.36

316	1.04	23.02	74.34	17.80
488	1.04	22.64	73.62	17.33
660	1.03	21.70	72.51	16.21
758	1.02	20.12	71.76	14.73
856	1.02	18.50	68.62	12.95
1000	1.01	16.31	65.80	10.84

Table S4. Summarized J-V characteristics of the α -In₂Se₃ based device without poling during the operational stability test. The curves were recorded at a scan rate of 0.01 V s⁻¹ in reverse mode.

Time (h)	V _{OC} (V)	J _{SC} (mA cm ⁻²)	FF (%)	PCE (%)
0	1.12	24.98	81.27	22.74
24	1.13	25.01	82.00	23.17
72	1.13	24.95	81.36	22.94
150	1.12	24.91	81.25	22.67
316	1.12	24.82	80.94	22.50
488	1.12	24.79	80.81	22.44
660	1.12	24.74	80.62	22.34
758	1.11	24.78	80.66	22.19
856	1.11	24.77	80.53	22.14
1000	1.11	24.74	80.32	22.06

Table S5. Summarized J-V characteristics of the α -In₂Se₃ based device after a positive poling during the operational stability test. The curves were recorded at a scan rate of 0.01 V s⁻¹ in reverse mode.

Time (h)	V _{OC} (V)	J _{SC} (mA cm ⁻²)	FF (%)	PCE (%)
0	1.16	25.08	83.35	24.25
24	1.16	25.02	83.21	24.15
72	1.16	24.96	83.22	24.10

150	1.15	24.91	83.16	23.82
316	1.15	24.88	82.98	23.74
488	1.16	24.83	82.76	23.84
660	1.15	24.78	82.73	23.58
758	1.15	24.75	82.68	23.53
856	1.14	24.73	82.67	23.31
1000	1.14	24.71	82.64	23.28
